

# MMGSD: Multi-Modal Gaussian Shape Descriptors for Correspondence Matching in 1D and 2D Deformable Objects

Aditya Ganapathi<sup>\*1</sup>, Priya Sundaresan<sup>\*1</sup>, Brijen Thananjeyan<sup>1</sup>, Ashwin Balakrishna<sup>1</sup>, Daniel Seita<sup>1</sup>, Ryan Hoque<sup>1</sup>, Joseph E. Gonzalez<sup>1</sup>, Ken Goldberg<sup>1</sup>

**Abstract**—We explore learning pixelwise correspondences between images of deformable objects in different configurations. Traditional correspondence matching approaches such as SIFT, SURF, and ORB can fail to provide sufficient contextual information for fine-grained manipulation. We propose Multi-Modal Gaussian Shape Descriptor (MMGSD), a new visual representation of deformable objects which extends ideas from dense object descriptors to predict all symmetric correspondences between different object configurations. MMGSD is learned in a self-supervised manner from synthetic data and produces correspondence heatmaps with measurable uncertainty. In simulation, experiments suggest that MMGSD can achieve an RMSE of 32.4 and 31.3 for square cloth and braided synthetic nylon rope respectively. The results demonstrate an average of 47.7% improvement over a provided baseline based on contrastive learning, symmetric pixel-wise contrastive loss (SPCL), as opposed to MMGSD which enforces distributional continuity.

## I. INTRODUCTION

Robotic manipulation of deformable objects is a growing area of research that has exposed many limitations in perception systems [1, 5, 6, 9–11, 15, 16, 18, 20]. Acquiring useful visual state representations of deformable objects for manipulation is a central focus in prior work [8, 13, 16, 17, 19, 21]. Inferring such representations is challenging due to the infinite dimensional state space, tendency to self-occlude, and often textureless and symmetric nature of deformable objects. One successful prior approach is learning pixelwise correspondences between images of deformable objects in different configurations as in Florence [3], Florence *et al.* [4], Ganapathi *et al.* [5], Javdani *et al.* [7], Schulman *et al.* [14], Sundaresan *et al.* [16], and Tang *et al.* [17]. However, these methods can fail to address uncertainty and symmetries, which can cause issues for downstream planning and control. Consider a robotic agent attempting to identify a corner of towel to fold it according to a video demonstration. The agent could leverage the fabric’s inherent symmetry to manipulate the corner of the towel for which its uncertainty in its location is the lowest, since all four corners are viable options. To enable such behaviors, we extend the correspondence learning algorithms from [4, 5, 16] to (1) provide measures of uncertainty in predicted correspondences by formulating a distribution matching objective for correspondence learning inspired by [3] and (2) explicitly predicting symmetric correspondences. Experiments suggest that the learned correspondences for both 1D and

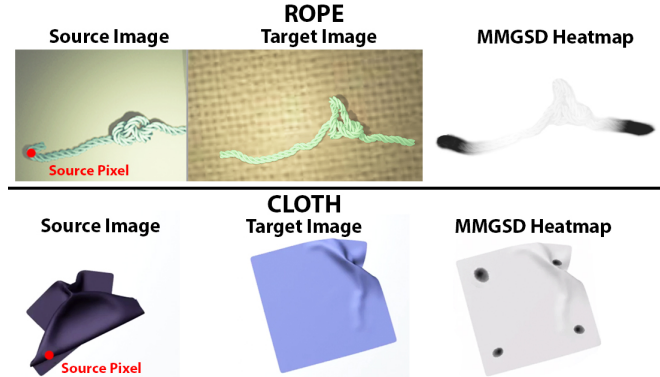


Fig. 1: Multi-Modal Gaussian Shape Descriptors (MMGSD) learns symmetry-aware pixelwise correspondences for multi-modal semantic keypoints between source and target images of deformable objects. We visualize the results of 2-modal and 4-modal MMGSD correspondence heatmaps for rope and cloth, respectively, relative to the source pixels from column 1.

2D deformable objects are more stable and continuous than those used in prior work and are less prone to symmetrical ambiguities and provide uncertainty estimates.

## II. PROBLEM STATEMENT

Given two images,  $I_a$  and  $I_b$ , of a deformable object in two different configurations respectively, and a source pixel location  $(u_a, v_a)$  (such that the pixel is  $I_a[u_a, v_a]$ ), find its  $n(u_a, v_a)$  pixel correspondences  $((u_{b_i}, v_{b_i}))_{i=1}^{n(u_a, v_a)}$  in  $I_b$ . There may be multiple possible matches due to symmetry, such as when matching a corner of a square cloth in  $I_a$  to all four corners of the cloth in  $I_b$ . We assume access to a dataset of pairs of images of deformable objects, for which  $n(u_a, v_a)$  is known, and a collection of correspondences and non-correspondences between each pair. We use Blender 2.8 [2] to both generate arbitrary configurations of cloth and rope in simulation as well as to render images of these configurations for dataset curation. Blender gives us access to the underlying mesh vertices that these objects are composed of which allows us to densely sample mesh vertex pixel locations at any point.

## III. METHODS

### A. Preliminaries: Pixel-wise Contrastive Loss

We first review the unimodal matching method from [4, 5, 12, 16]. A neural network  $f$  maps  $I_a$  to a  $D$ -dimensional descriptor volume:  $f : \mathbb{R}^{W \times H \times 3} \mapsto \mathbb{R}^{W \times H \times D}$ . During training, a pair of images and sets of both matching pixels and non-matching pixels are sampled between the image pair. The following contrastive loss minimizes descriptor distance between matching pixels and pushes descriptors for non-matching pixels apart by a fixed margin  $M$ :

<sup>\*</sup> Authors have contributed equally and names are in alphabetical order.

<sup>1</sup>University of California, Berkeley, USA

Correspondence to Aditya Ganapathi: avganapathi@berkeley.edu

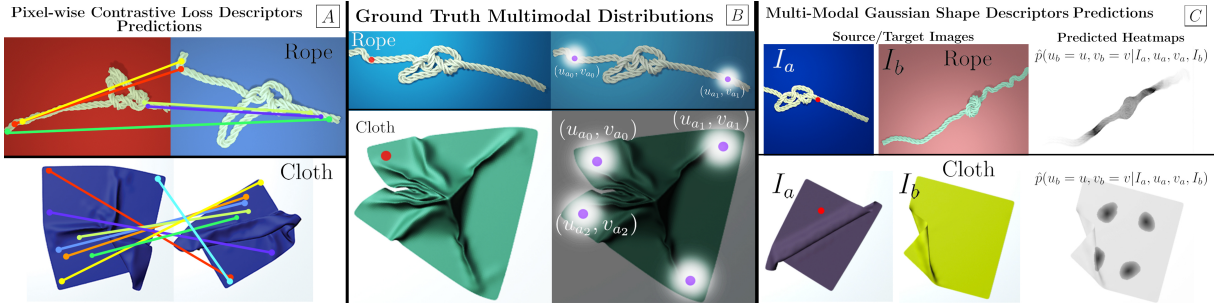


Fig. 2: We visualize the multi-modal ground truth distributions (B) and predicted (A,C) correspondences on domain-randomized images of both cloth and rope. Contrastive descriptor-based methods can fail to generalize to objects with inherent symmetries, as in example A. In contrast, the predicted 2-modal and 4-modal MMGSD heatmaps for rope and cloth, respectively, appear to be sensitive to object symmetries. MMGSD exhibits the least uncertainty at object extremities and greater variance as the source pixel moves inward (C), as shown in the probability mass distributed around the rope knot (top heatmap of C).

$$L(I_a, I_b, u_a, v_a, u_b, v_b) = \begin{cases} \|f(I_b)[u_b, v_b] - f(I_a)[u_a, v_a]\|_2^2 & \text{match} \\ \max(0, M - \|f(I_b)[u_b, v_b] - f(I_a)[u_a, v_a]\|_2)^2 & \text{non-match} \end{cases}$$

While this method is effective at determining pixel-wise correspondences for both cloth and rope [5, 16], it does not account for inherent symmetry in these objects and therefore is susceptible to symmetric orientation based error as is shown in the 2D cloth example of Figure 2B. The authors of [5] address this by limiting the rotation of the training data for a square fabric to be between  $(-\frac{\pi}{4}, -\frac{\pi}{4})$ , but the model still suffers from symmetric ambiguities at the boundary conditions. The authors of [16] break symmetry by adding a ball to the end of the rope.

### B. Symmetric Pixel-wise Contrastive Loss (SPCL) Baseline

This method extends Section III-A to handle multiple matches for the same source pixel  $(u_a, v_a)$ . Now, we try to match equivalent source pixels  $((u_{a_i}, v_{a_i}))_{i=0}^n$  to a set of destination pixels  $((u_{b_i}, v_{b_i}))_{i=0}^n$  that are equivalent due to symmetry by adding all pairs of pixels as matches. We use the same loss function as in Section III-A.

While this method addresses the symmetry issue from method III-A by learning to find multiple matches in the destination image for an input pixel, we find that it is unstable and has discontinuity issues due to the contrastive nature of training. During test time, we create a heatmap of the target image by normalizing the descriptor norm differences. We then fit an  $n(u_a, v_a)$ -modal Gaussian distribution to the heatmap and take the  $n(u_a, v_a)$  pixel modes as the predicted symmetric correspondences.

### C. Symmetric Distributional Loss (MMGSD)

We extend a distributional descriptor network method suggested in [3] to learn an estimator  $\hat{p}(u_b = u, v_b = v | I_a, u_a, v_a, I_b)$  that outputs the probability that  $(u, v)$  in  $I_b$  matches with  $(u_a, v_a)$  in  $I_a$ . Specifically, we let  $\hat{p}(u_b = u, v_b = v | I_a, u_a, v_a, I_b) = \frac{\exp\|f(I_a)[u_a, v_a] - f(I_b)[u, v]\|_2^2}{\sum_{u', v'} \exp\|f(I_a)[u_a, v_a] - f(I_b)[u', v']\|_2^2}$ , where  $f$  is a neural network with trainable parameters. To fit  $\hat{p}$ , we use the cross-entropy loss function with respect to a target distribution  $p$  that is an isotropic Gaussian mixture model with modes

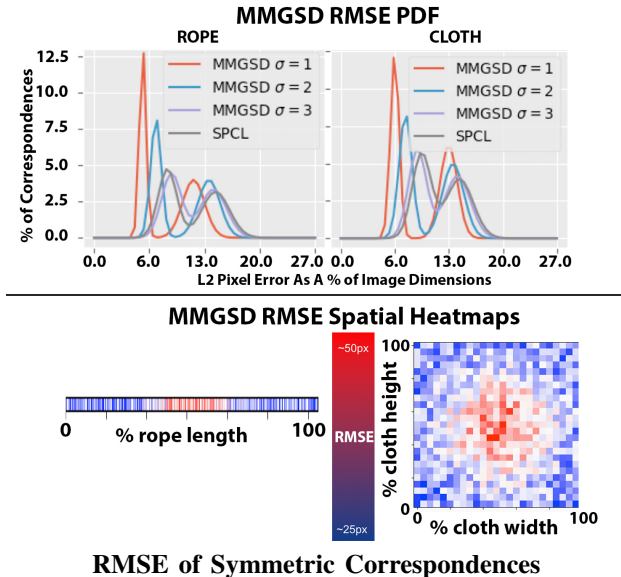
at all the ground truth pixel correspondences in  $I_b$ , thus accounting for all symmetric matches. For the ground truth target distributions,  $\sigma$  is empirically fine-tuned to tradeoff spatial continuity in the learned distribution with overlap and collapse of modes. Using this distributional divergence loss function maintains spatial continuity between matches, and we find that this can be more stable than the method in Section III-B. Additionally, predicting a distribution instead allows uncertainty estimation by computing the entropy of the predicted distribution. This method is similar to [3] but uses a multi-modal target distribution due to the multiple symmetric correspondences. As illustrated in Figure 2B and Figure 1B, this method is successfully able to place its mass at the multiple possible matches in the target image. We fit an  $n(u_a, v_a)$ -modal Gaussian distribution to the predicted output distribution  $\hat{p}$  and take the  $n(u_a, v_a)$  pixel modes as the predicted symmetric correspondences.

## IV. QUANTITATIVE RESULTS

We evaluate the quality of the symmetric learned correspondences (methods III-B and III-C) using the root-mean-square error (RMSE) metric. Both the rope and cloth networks are trained on 3,500 training images each and evaluated on a held-out test set of 500 images. All training and testing is carried out with images of a synthetic square cloth and braided synthetic nylon rope. The cloth images are  $485 \times 485$  and the rope images are  $640 \times 480$  in aspect ratio. We compute the  $n(u_a, v_a)$  pixel mode predictions and compare them directly to the ground truth pixel locations:  $\frac{1}{n(u_a, v_a)} \sum_{i=1}^{n(u_a, v_a)} \|\hat{u}_{b_i}, \hat{v}_{b_i} - [u_{b_i}, v_{b_i}]\|_2^2$  where  $[u_{b_i}, v_{b_i}]$  is the ground truth pixel correspondence in  $I_b$  for the source pixel  $[u_a, v_a]$ . We average over 625 source pixel locations in each of 500 test image pairs from simulation (Figure 3) using a model trained on 3500 image pairs of cloth and rope each.

In Figure 3 we compare MMGSD against SPCL with the probability density function of percentage of correspondences below an L2 pixel threshold (as a percentage of the pixel dimensions of the object). We note that while MMGSD is able to predict multi-modal correspondences more effectively than SPCL, it exhibits high uncertainty and modal collapse for highly occluded regions, such as rope knots (Figure 2C), object interiors, or occluded fabric corners. This high

degree of variance in the resulting heatmaps is a consequence of MMGSD attempting to preserve spatial continuity, at the expense of concentrating probability mass in isolated symmetric regions. We illustrate this in the bottom half of Figure 3 by visualizing the source of high RMSE error on both rope and cloth. The top half of Figure 3 also reveals this second mode centered at higher RMSE error.



### RMSE of Symmetric Correspondences

Fig. 3: We find that MMGSD, trained with  $\sigma = 1\text{px}$ , is able to more effectively learn symmetric correspondences over SPCL, evaluated by the PDF of correspondences with respect to L2 pixel error. For all other  $\sigma$ , MMGSD degrades due to intermixing of modes caused by higher variance in the ground truth target distributions. We also visualize the average RMSE in 1D and 2D space for rope and cloth, respectively, noting that MMGSD exhibits the highest error at object interiors due to modal collapse and relatively low RMSE at object extremities. This behavior of MMGSD is also suggested by the bimodal nature of the PDF with low error at object exteriors (first peak) and higher error at object interiors (second peak).

## V. DISCUSSION AND FUTURE WORK

This paper proposes an extension of dense descriptor-based pixel-wise correspondence that addresses symmetry and uncertainty estimation in deformable object tracking. In future work, we will explore generalizing MMGSD to other types of objects with task-relevant multimodal properties such as sleeves, buttons, drawstrings, or pockets on clothing. We hypothesize that the uncertainty of MMGSD — in object interiors or in occluded parts — would pose a challenge to tasks that involve manipulating all parts of a deformable object, such as untying a knotted rope or performing consecutive folds on a fabric. However, we will further investigate the limitations of MMGSD and ways to utilize these measures of uncertainty while planning, such as by taking actions to disambiguate a deformable object’s state. The framework presented is also applicable to rigid objects containing an axis of symmetry or multimodal properties. Additionally, we will explore learning the dynamics of these correspondences conditioned on robot action sequences. We will also explore 3D representations of deformable objects using geodesic distance as a measure of correspondence.

## VI. ACKNOWLEDGMENTS

This research was performed at the AUTOLAB at UC Berkeley in affiliation with the Berkeley AI Research (BAIR) Lab with partial support from Toyota Research Institute. Any opinions, findings, and conclusions or recommendations expressed in this material are those of the author(s) and do not necessarily reflect the views of the sponsors. Ashwin Balakrishna is supported by an NSF GRFP and Daniel Seita is supported by an NPSC Fellowship.

## REFERENCES

- [1] C. Chi and D. Berenson, “Occlusion-robust deformable object tracking without physics simulation”, in *2019 IEEE/RSJ International Conference on Intelligent Robots and Systems (IROS)*, IEEE, 2019, pp. 6443–6450.
- [2] B. O. Community, *Blender - a 3D modelling and rendering package*, Blender Foundation, Stichting Blender Foundation, Amsterdam, 2018.
- [3] P. R. Florence, Ph.D. dissertation, Massachusetts Institute of Technology, 2020.
- [4] P. R. Florence, L. Manuelli, and R. Tedrake, “Dense Object Nets: Learning Dense Visual Object Descriptors By and For Robotic Manipulation”, in *Conf. on Robot Learning (CoRL)*, 2018.
- [5] A. Ganapathi, P. Sundaresan, B. Thananjeyan, A. Balakrishna, D. Seita, J. Grannen, M. Hwang, R. Hoque, J. E. Gonzalez, N. Jamali, *et al.*, “Learning to Smooth and Fold Real Fabric Using Dense Object Descriptors Trained on Synthetic Color Images”, *arXiv preprint arXiv:2003.12698*, 2020.
- [6] R. Hoque, D. Seita, A. Balakrishna, A. Ganapathi, A. Tanwani, N. Jamali, K. Yamane, S. Iba, and K. Goldberg, “VisuoSpatial Foresight for Multi-Step, Multi-Task Fabric Manipulation”, in *Proc. Robotics: Science and Systems (RSS)*, 2020.
- [7] S. Javdani, S. Tandon, J. Tang, J. F. O’Brien, and P. Abbeel, “Modeling and perception of deformable one-dimensional objects”, in *2011 IEEE International Conference on Robotics and Automation*, IEEE, 2011, pp. 1607–1614.
- [8] J. Matas, S. James, and A. J. Davison, “Sim-to-Real Reinforcement Learning for Deformable Object Manipulation”, in *Conf. on Robot Learning (CoRL)*, 2018.
- [9] D. McConachie and D. Berenson, “Estimating model utility for deformable object manipulation using multiarmed bandit methods”, *IEEE Transactions on Automation Science and Engineering*, vol. 15, no. 3, pp. 967–979, 2018.
- [10] A. Nair, D. Chen, P. Agrawal, P. Isola, P. Abbeel, J. Malik, and S. Levine, “Combining Self-Supervised Learning and Imitation for Vision-Based Rope Manipulation”, in *Proc. IEEE Int. Conf. Robotics and Automation (ICRA)*, 2017.
- [11] J. Qian, T. Weng, L. Zhang, B. Okorn, and D. Held, “Cloth Region Segmentation for Robust Grasp Selection”, in *Proc. IEEE/RSJ Int. Conf. on Intelligent Robots and Systems (IROS)*, 2020.
- [12] T. Schmidt, R. A. Newcombe, and D. Fox, “Self-Supervised Visual Descriptor Learning for Dense Correspondence”, *IEEE Robotics and Automation Letters*, vol. 2, pp. 420–427, 2017.
- [13] J. Schulman, J. Ho, C. Lee, and P. Abbeel, “Learning from demonstrations through the use of non-rigid registration”, in *Robotics Research*, Springer, 2016, pp. 339–354.
- [14] J. Schulman, A. Lee, J. Ho, and P. Abbeel, “Tracking deformable objects with point clouds”, in *2013 IEEE International Conference on Robotics and Automation*, IEEE, 2013, pp. 1130–1137.
- [15] D. Seita, A. Ganapathi, R. Hoque, M. Hwang, E. Cen, A. K. Tanwani, A. Balakrishna, B. Thananjeyan, J. Ichnowski, N. Jamali, K. Yamane, S. Iba, J. Canny, and K. Goldberg, “Deep Imitation Learning of Sequential Fabric Smoothing From an Algorithmic Supervisor”, in *Proc. IEEE/RSJ Int. Conf. on Intelligent Robots and Systems (IROS)*, 2020.

- [16] P. Sundaresan, J. Grannen, B. Thananjeyan, A. Balakrishna, M. Laskey, K. Stone, J. E. Gonzalez, and K. Goldberg, “Learning Rope Manipulation Policies using Dense Object Descriptors Trained on Synthetic Depth Data”, in *Proc. IEEE Int. Conf. Robotics and Automation (ICRA)*, 2020.
- [17] T. Tang, Y. Fan, H.-C. Lin, and M. Tomizuka, “State estimation for deformable objects by point registration and dynamic simulation”, in *2017 IEEE/RSJ International Conference on Intelligent Robots and Systems (IROS)*, IEEE, 2017, pp. 2427–2433.
- [18] B. Thananjeyan, A. Garg, S. Krishnan, C. Chen, L. Miller, and K. Goldberg, “Multilateral Surgical Pattern Cutting in 2D Orthotropic Gauze with Deep Reinforcement Learning Policies for Tensioning”, in *Proc. IEEE Int. Conf. Robotics and Automation (ICRA)*, 2017.
- [19] A. Wang, T. Kurutach, K. Liu, P. Abbeel, and A. Tamar, “Learning robotic manipulation through visual planning and acting”, in *Proc. Robotics: Science and Systems (RSS)*, 2019.
- [20] Y. Wu, W. Yan, T. Kurutach, L. Pinto, and P. Abbeel, “Learning to Manipulate Deformable Objects without Demonstrations”, in *Proc. Robotics: Science and Systems (RSS)*, 2020.
- [21] M. Yan, Y. Zhu, N. Jin, and J. Bohg, “Self-Supervised Learning of State Estimation for Manipulating Deformable Linear Objects”, *IEEE Robotics and Automation Letters*, vol. 5, no. 2, pp. 2372–2379, 2020.